Supplement of Atmos. Meas. Tech., 16, 4643–4665, 2023
https://doi.org/10.5194/amt-16-4643-2023-supplement

Atmospheric Measurement Techniques
Open Access

Supplement of

A research product for tropospheric NO_2 columns from Geostationary Environment Monitoring Spectrometer based on Peking University OMI NO_2 algorithm

Yuhang Zhang et al.

Correspondence to: Jintai Lin (linjt@pku.edu.cn)

1. Derivation of the assumption in the total NO_2 SCD correction method

In principle, the corrected total NO_2 SCDs by combining GEMS and TROPOMI observations should be:

$$\mathrm{SCD}_{\mathrm{total},h}^{\mathrm{corrected}} = \mathrm{SCD}_{\mathrm{total},h}^{\mathrm{GEMS}} + \left(\frac{\mathrm{SCD}_{\mathrm{total},h}^{\mathrm{TROPOMI}}}{\mathrm{AMF}_{\mathrm{total},h}^{\mathrm{TROPOMI}}} - \frac{\mathrm{SCD}_{\mathrm{total},h}^{\mathrm{GEMS}}}{\mathrm{AMF}_{\mathrm{total},h}^{\mathrm{GEMS}}}\right) \cdot \mathrm{AMF}_{\mathrm{total},h}^{\mathrm{GEMS}}$$

$$= \mathrm{SCD}_{\mathrm{total},h}^{\mathrm{TROPOMI}} \cdot \frac{\mathrm{AMF}_{\mathrm{total},h}^{\mathrm{GEMS}}}{\mathrm{AMF}_{\mathrm{total},h}^{\mathrm{TROPOMI}}}$$

$$= \mathrm{SCD}_{\mathrm{total},h}^{\mathrm{TROPOMI}} \cdot \frac{\mathrm{AMFgeo}_{h}^{\mathrm{GEMS}} \int_0^\infty w_{\mathrm{h}}^{\mathrm{GEMS}}(z) S(z) \mathrm{d}z}{\mathrm{AMFgeo}_{h}^{\mathrm{TROPOMI}} \int_0^\infty w_{\mathrm{h}}^{\mathrm{TROPOMI}}(z) S(z) \mathrm{d}z}$$

$$= \mathrm{SCD}_{\mathrm{total},h}^{\mathrm{TROPOMI}} \cdot \frac{\mathrm{AMFgeo}_{h}^{\mathrm{GEMS}} \left(\int_{z_\mathrm{T}}^\infty w_{h}^{\mathrm{GEMS}}(z) S(z) \mathrm{d}z + \int_0^{z_\mathrm{T}} w_{h}^{\mathrm{GEMS}}(z) S(z) \mathrm{d}z\right)}{\mathrm{AMFgeo}_{h}^{\mathrm{TROPOMI}} \left(\int_{z_\mathrm{T}}^\infty w_{h}^{TROPOMI}(z) S(z) \mathrm{d}z + \int_0^{z_\mathrm{T}} w_{h}^{\mathrm{TROPOMI}}(z) S(z) \mathrm{d}z\right)}$$

$$\approx \mathrm{SCD}_{\mathrm{total},h}^{\mathrm{TROPOMI}} \cdot \frac{\mathrm{AMFgeo}_{h}^{\mathrm{GEMS}} \left(1 + \int_0^{z_\mathrm{T}} w_{h}^{\mathrm{GEMS}}(z) S(z) \mathrm{d}z\right)}{\mathrm{AMFgeo}_{h}^{\mathrm{TROPOMI}} \left(1 + \int_0^{z_T} w_{h}^{\mathrm{TROPOMI}}(z) S(z) \mathrm{d}z\right)}$$

$$= \mathrm{SCD}_{\mathrm{total},h}^{\mathrm{TROPOMI}} \cdot \frac{\mathrm{AMFgeo}_{h}^{\mathrm{GEMS}}}{\mathrm{AMFgeo}_{h}^{\mathrm{TROPOMI}}} \cdot \frac{1 + \frac{\mathrm{AMF}_{h}^{\mathrm{GEMS}}}{\mathrm{AMFgeo}_{h}^{\mathrm{GEMS}}}}{1 + \frac{\mathrm{AMF}_{h}^{\mathrm{TROPOMI}}}{\mathrm{AMFgeo}_{h}^{\mathrm{TROPOMI}}}}$$

In our actual correction, we define and assume the "approximation ratio" as:

$$\frac{1 + \frac{\mathrm{AMF}_{h}^{\mathrm{GEMS}}}{\mathrm{AMFgeo}_{h}^{\mathrm{GEMS}}}}{1 + \frac{\mathrm{AMF}_{h}^{\mathrm{TROPOMI}}}{\mathrm{AMFgeo}_{h}^{\mathrm{TROPOMI}}}} \approx 1$$

So that the corrected NO_2 SCDs become:

$$\mathrm{SCD}_{\mathrm{total},h}^{\mathrm{corrected}} = \mathrm{SCD}_{\mathrm{total},h}^{\mathrm{TROPOMI}} \cdot \frac{\mathrm{AMFgeo}_{h}^{\mathrm{GEMS}}}{\mathrm{AMFgeo}_{h}^{\mathrm{TROPOMI}}}$$

Figure S2 shows the spatial distribution of mean "approximation ratio" in June 2021 which we assume to be 1. The "approximation ratio" is in the range of 0.9 – 1.1 in most central and eastern parts of GEMS FOV, but is smaller in the western and northwestern parts (around 0.8 in most places, with a minimum value around 0.7).

2. MAX-DOAS instruments

There are four instruments installed in various areas of Shanghai. The instrument located in the campus of Fudan University is in the urban center of Shanghai (31.34°N, 121.52°E). The telescope's azimuth angle is 0°, and the scattered sunlight is measured at ten elevation angles of 2°, 3°, 5°, 7°, 10°, 15°, 20°, 30°, 45° and 90° within 15 minutes. The Nanhui site is in the suburban area (31.06°N, 121.80°E) and about 10 km southeast to the center of Shanghai. The azimuth angle is set to 2° and it takes about 15 minutes for a full cycle with elevation angles of 2°, 3°, 5°, 7°, 9°, 12°, 15°, 20°, 30°, 45° and 90°. The Dianshan Lake site is located near the Dianshan Lake Scenic Area (31.10°N, 120.98°E), which is at the junction of Suzhou and Shanhai. The Chongming site is on the Chongming Island (31.50°N, 121.82°E) of Shanghai, which is China's third largest island and located in Yangtze River estuary. The instruments at Dianshan Lake (suburban) and Chongming (rural) sites are operated in the same way as that in the Nanhui site, except with a fixed azimuth angle at 5° (Zhang et al., 2021; Zhang et al., 2022a; Zhang et al., 2022b; Zhu et al., 2022).

The instrument operated in Xianghe is designed by BIRA-IASB and run by both BIRA-IASB and CAS-IAP. It is located in the suburban area (39.75°N, 116.96°E) of Xianghe county to the southwest of Beijing. The telescope's azimuth direction is fixed to the north, and a full scan requiring about 15 minutes comprises nine elevation angles: 2°, 4°, 6°, 8°, 10°, 12°, 15°, 30° and 90°(Clémer et al., 2010; Hendrick et al., 2014).

The instrument in Xuzhou is set on the roof of the School of Environmental Science and Spatial Informatics, China University of Mining and Technology (34.22°N, 117.14°E). It is located 6.5 km away from the urban center of Xuzhou, and about 1 km south to the Yunlong Lake Scenic Area, which is a 5A natural scenic area. It measures scattered sunlight every 5 minutes for five zenith angles: 5°, 10°, 20°, 30° and 90°. This instrument is normally operated from 9:00 to 17:00 local solar time (LST) each day (Liu et al., 2020).

The instrument in Hefei site was deployed in March 2008 and is run by Anhui Institute of Optics and Fine Mechanics (AIOFM), Chinese Academy of Science (CAS). It is located outdoors in the campus of AIOFM and about 10 km northwest to the center of Hefei city (31.91°N, 117.16°E). It takes 30 minutes for a cycle to measure introduced scattered sunlight with sequential elevation angles of 3°, 5°, 10°, 20°, 30° and 90° (Kanaya et al., 2014).

The Fukue and Cape Hedo sites are both remote sites located far away from the major cities (32.75°N, 128.68°E and 26.87°N, 128.25°E, respectively). They are suitable for monitoring tropospheric NO2 in the background regions and outflow from Korea and China. Similar to the instrument at Hefei, the scattered sunlight is measured by rotating a prism at six elevation angles 3°, 5°, 10°, 20°, 30° and 90°, with 5 minutes for each angle and 30 minutes for a total (Kanaya et al., 2014; Choi et al., 2021).

3. Discussion of the differences between POMINO-GEMS and POMINO-TROPOMI v1.2.2 tropospheric NO_2 VCDs

The differences between POMINO-GEMS and POMINO-TROPOMI v1.2.2 tropospheric NO_2 VCDs are related to tropospheric NO_2 AMFs and SCDs. As shown in Figure S10, POMINO-GEMS tropospheric NO_2 AMF is larger than POMINO-TROPOMI v1.2.2 in the western part of GEMS FOV, except over major cities such as Urumqi in China and New Delhi in India, but is smaller in most of the eastern part. Such AMF differences can be further separated into differences in geometric AMF and scattering correction factor.

For a certain pixel and time, GEMS and TROPOMI have the same SZA but different VZAs and thus different geometric AMFs. The GEMS geometric AMFs exhibit a circle-like spatial pattern, increasing from less than 3 in the southeast to more than 5 in the northwest of GEMS FOV, corresponding to the increase of VZA. In contrast, the TROPOMI geometric AMFs exhibit a different spatial pattern with values varying from 2 to 3 (Figure S11). As a result, the GEMS geometric AMFs are larger than those of TROPOMI in the northwest and smaller in the southeast of GEMS FOV.

The scattering correction factors of POMINO-GEMS and POMINO-TROPOMI v1.2.2 are different as well. POMINO-GEMS explicitly employs CALIOP-corrected aerosol vertical profiles and re-calculates cloud fraction and cloud pressure based on continuum reflectances and O_2-O_2 SCDs from GEMS observations. By comparison, POMINO-TROPOMI v1.2.2 does not use CALIOP observations to constrain aerosol vertical profiles; and it takes the FRESCO-wide cloud pressure data from the official TROPOMI PAL v2.3.1 NO_2 product and re-calculates cloud fraction at 440 nm. Constraint by CALIOP observations results in higher aerosol-concentrated layer heights (Liu et al., 2019), which enhances the "screening" effect on the absorption by NO_2 and leads to lower scattering correction factors over polluted regions such as eastern China (Figure S12). Higher scattering correction factors of POMINO-GEMS occur over remote areas such as the Pacific Ocean.

In addition to tropospheric NO_2 AMFs, the differences in tropospheric NO_2 SCDs between POMINO-GEMS and POMINO-TROPOMI v1.2.2 also contribute to their differences in VCDs. In the correction for total NO_2 SCDs, the corrected total GCDs of GEMS are forced to agree with TROPOMI

PAL v2.3.1 GCDs at the overpass time of TROPOMI. Thus, the difference in geometry between GEMS and TROPOMI leads to different total NO_2 SCDs and hence tropospheric SCDs. In Figure S13c and d, the spatial distribution of differences in tropospheric NO_2 SCDs between POMINO-GEMS and POMINO-TROPOMI v1.2.2 shows positive values over northwestern part and negative values over southeastern part of GEMS FOV.

4. Supplemental tables and figures

Table S1. Basic information of TROPOMI, OMI, GOME-2 and GEMS instruments

Instrument	Spacecraft	Equator crossing time	Spectral range	Nominal spatial resolution
TROPOMI	Sentinel-5 Precursor (ESA)	13:30 LT	270-500 nm; 675-775 nm; 2305-2385 nm	3.5 × 7 km^2 (3.5 × 5.5 km^2 since 6th Aug. 2019)
OMI	EOS-Aura (NASA)	13:45 LT	270-500 nm	13 × 24 km^2
GOME-2	MetOp-A (EUMETSAT)	9:30 LT	240-790 nm	80 × 40 km^2
GEMS	Geostationary Korea Multi-Purpose Satellite-2B (GK-2B)	128.2°E over the equator	300-500 nm	7 × 8 km^2 (gases); 3.5 × 8 km^2 (aerosols)

Table S2. Specifics for the NO_2 SCD retrieval of TROPOMI PAL v2.3.1 and GEMS v1.0 operational products

	TROPOMI PAL v2.3.1	GEMS v1.0
Type of DOAS fit	Intensity fit	Optical fit
χ^2 minimization method	Levenberg-Marquardt	Levenberg-Marquardt
Wavelength range	405-465 nm	432-450 nm
Solar reference spectrum	E_{ref} from Chance and Kurucz (2010)	E_{ref} from Chance and Kurucz (2010)
NO_2 reference spectrum	σ_{NO_2} at 220 K from Vandaele et al. (1998)	σ_{NO_2} at 220 K from Vandaele et al. (1998)
O_3 reference spectrum	σ_{O_3} at 243 K from Serdyuchenko et al. (2014)	σ_{O_3} from 243 and 293 K from Bogumil et al. (2003)
O_2-O_2 reference spectrum	$\sigma_{O_2-O_2}$ at 293 K from Thalman and Volkamer (2013)	$\sigma_{O_2-O_2}$ at 293 K from Thalman and Volkamer (2013)
Water vapor reference spectrum	$\sigma_{H_2O_{vap}}$ at 293 K from	Not yet applied

	HITRAN 2012 data	
Liquid water reference spectrum	$\sigma_{H_2O_{liq}}$ from Pope and Fry (1997)	Not yet applied
Ring reference spectrum	I_{ring} derived following Chance and Spurr (1997)	σ_{ring} derived following Chance and Spurr (1997)

Table S3. Ground based MAX-DOAS measurements

Site name	Type	Geolocation	Measurement time
Fudan University	Urban	121.52°E, 31.34°N	1 June – 31 August 2021
Xuzhou	Suburban	117.14°E, 34.22°N	1 June – 31 August 2021
Hefei	Suburban	117.16°E, 31.91°N	1 June – 30 June 2021
Nanhui	Suburban	121.80°E, 31.06°N	1 June – 31 August 2021
Xianghe	Suburban	116.96°E, 39.75°N	1 June – 31 August 2021
Dianshan Lake	Suburban	120.98°E, 31.30°N	1 June – 31 August 2021
Chongming	Rural	121.82°E, 31.50°N	1 June – 31 August 2021
Fukue	Remote	128.68°E, 32.75°N	1 June – 31 August 2021
Cape Hedo	Remote	128.25°E, 26.87°N	1 June – 31 August 2021

Table S4. Evaluation of surface NO_2 concentrations derived from POMINO-GEMS with total

SCD correction and POMINO-GEMS without correction using MEE measurements

MEE sites	POMINO-GEMS with total SCD correction		POMINO-GEMS without total SCD correction	
	R	NMB	*R*	NMB
All	0.97	−34.4%	0.97	−27.1%
Urban	0.97	−28.7%	0.97	−19.8%
Suburban	0.97	−42.8%	0.97	−38.0%
Rural	0.96	−48.4%	0.96	−44.4%

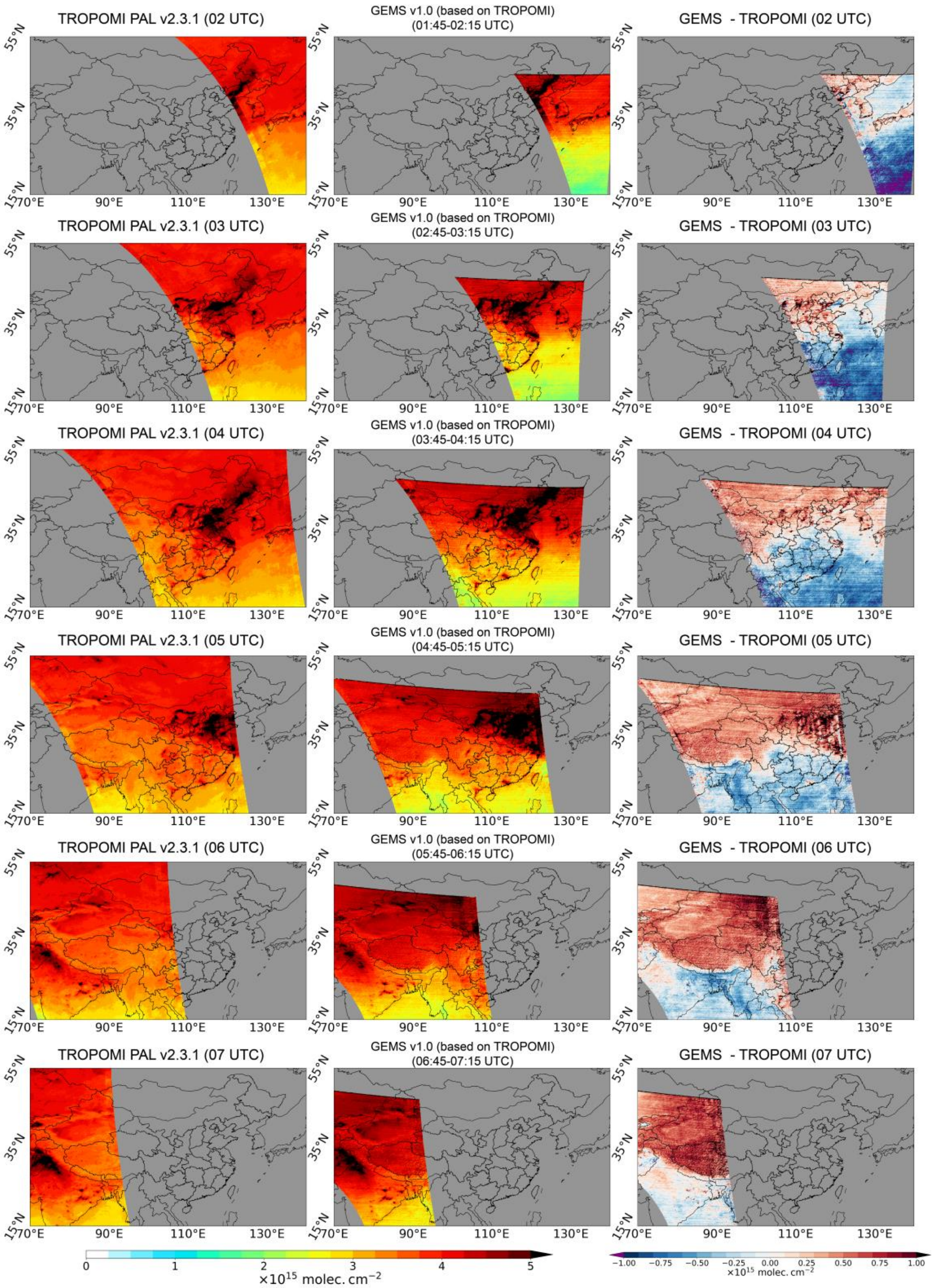

Figure S1. Spatial distribution of monthly mean total NO_2 GCDs at each hour on a 0.05° × 0.05° grid in June 2021. Left column, TROPOMI PAL v2.3.1 product; middle column, GEMS v1.0 product that spatiotemporally matches with TROPOMI; right column, the absolute differences of GEMS total NO_2 GCDs from those of TROPOMI. The regions in grey mean there are no valid observations.

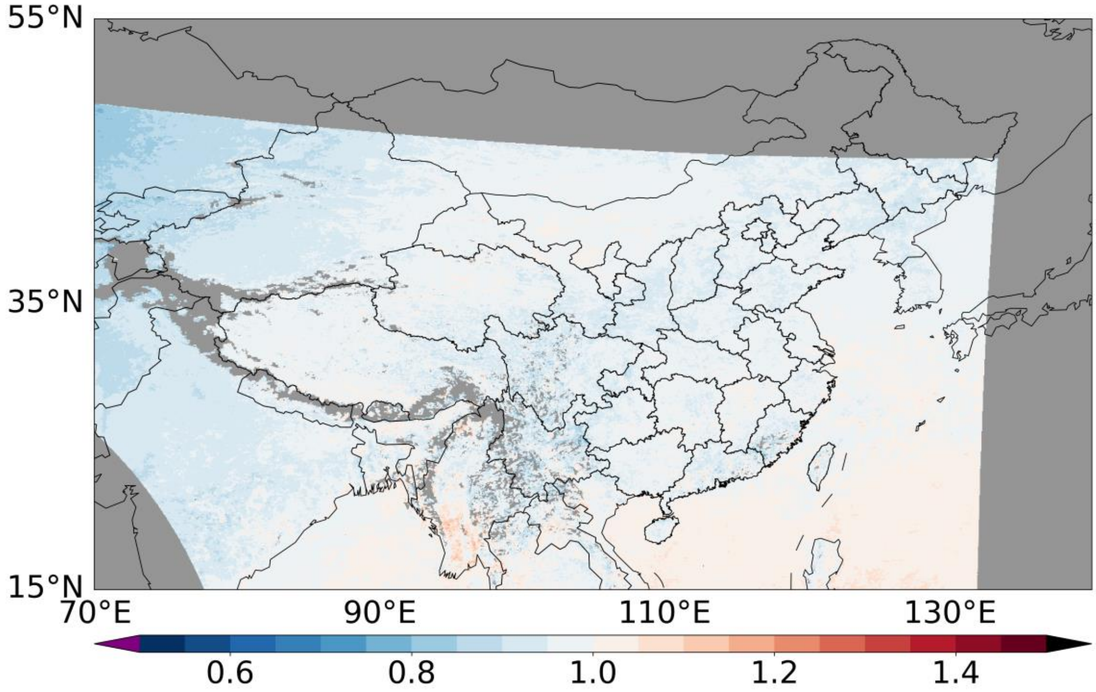

Figure S2. Spatial distribution of mean approximation ratios on a 0.05° × 0.05° grid in June 2021. The regions in grey mean there are no valid NO_2 observations.

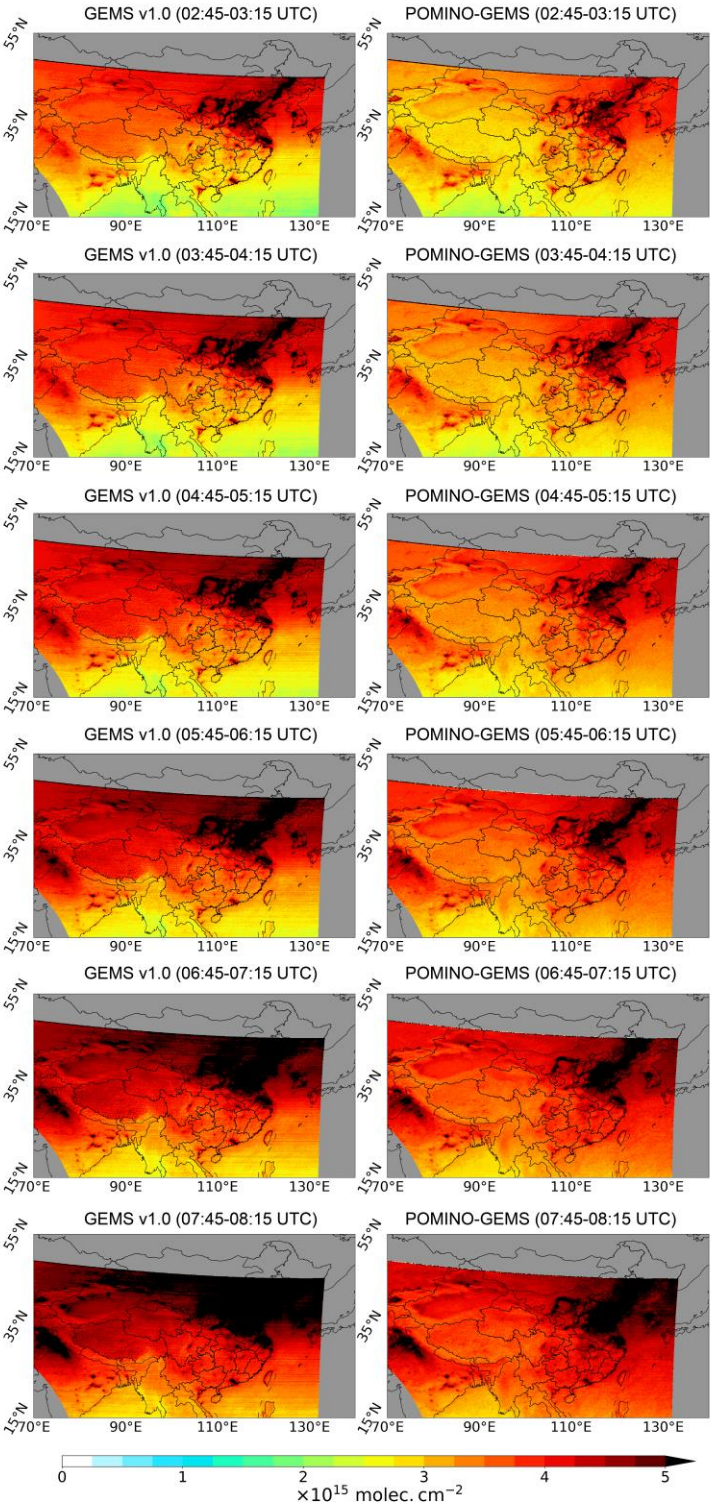

Figure S3. Spatial distribution of monthly mean total NO_2 GCDs at each hour on a 0.05° × 0.05° grid in June 2021. Left column, official GEMS v1.0 product; right column, corrected POMINO-GEMS product. The regions in grey mean there are no valid observations.

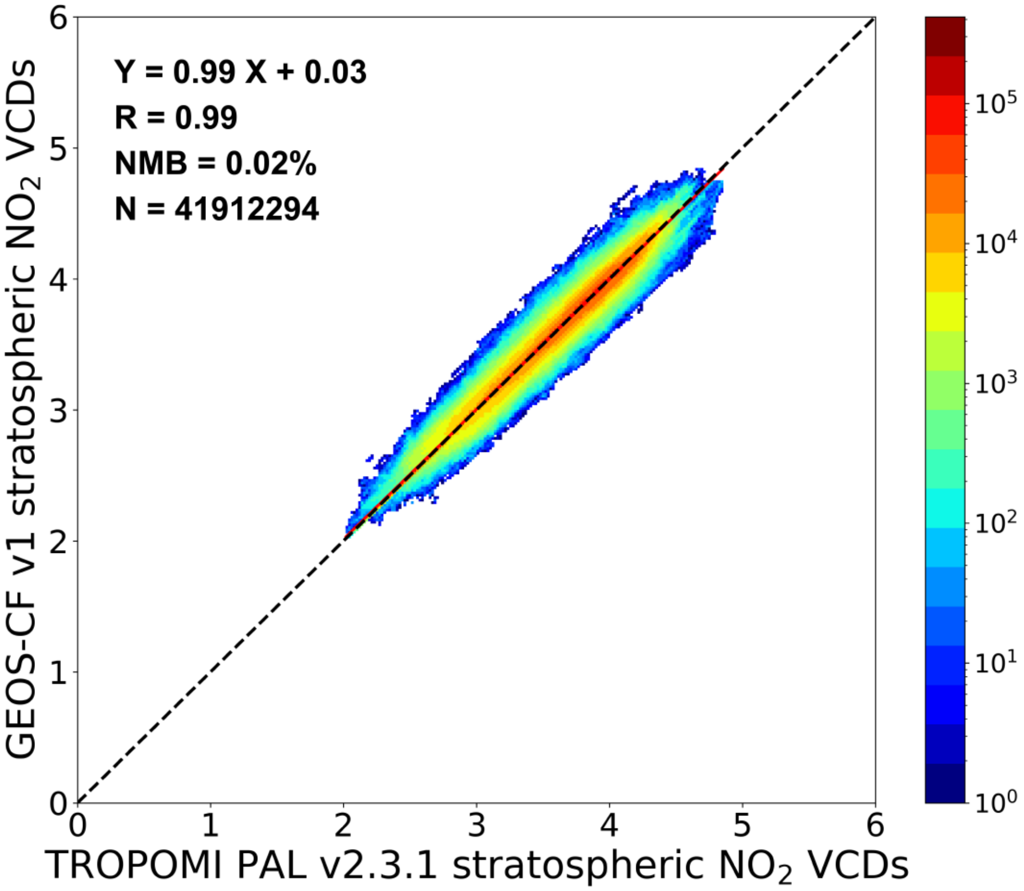

Figure S4. Scatterplot for stratospheric NO_2 VCDs between GEOS-CF v1 and TROPOMI PAL v2.3.1 products in June 2021. Colors represent the data density.

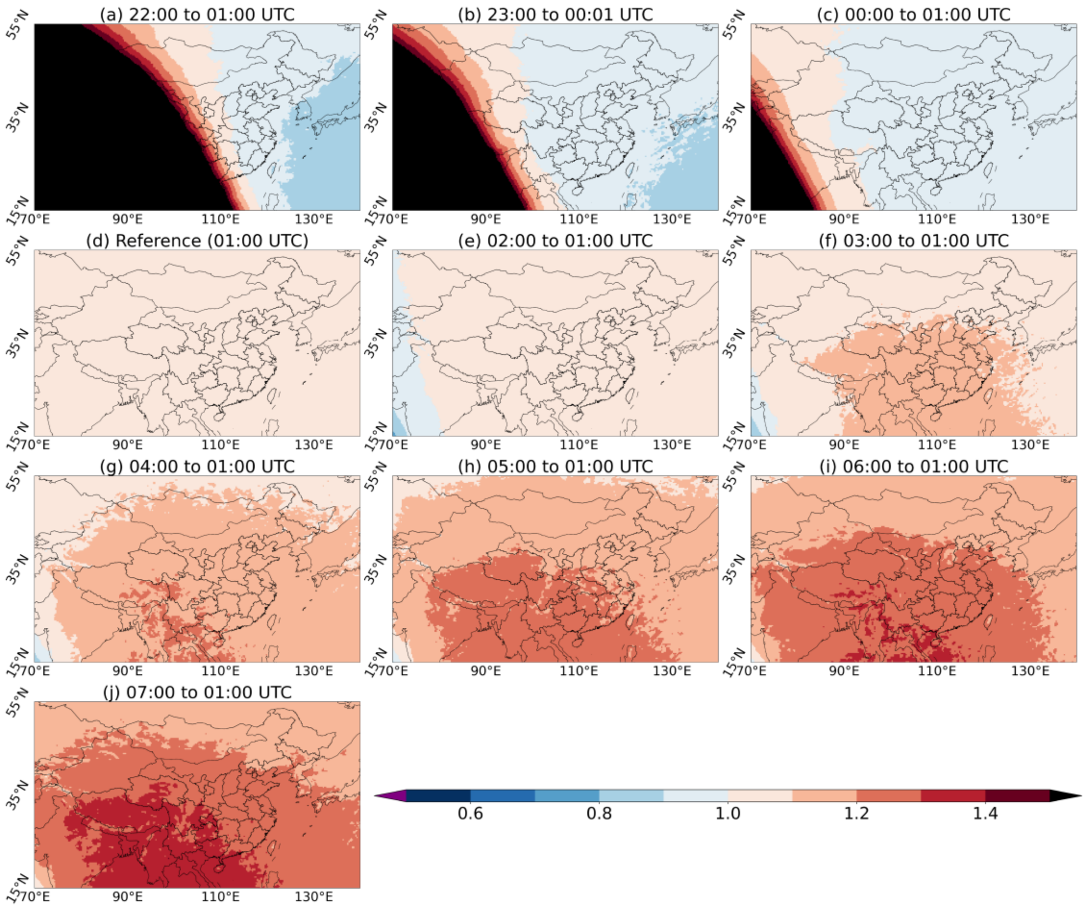

Figure S5. Spatial distribution of GEOS-CF derived stratospheric NO_2 ratio at each hour to the reference hour (01:00 UTC) on a 0.05° × 0.05° grid in June 2021.

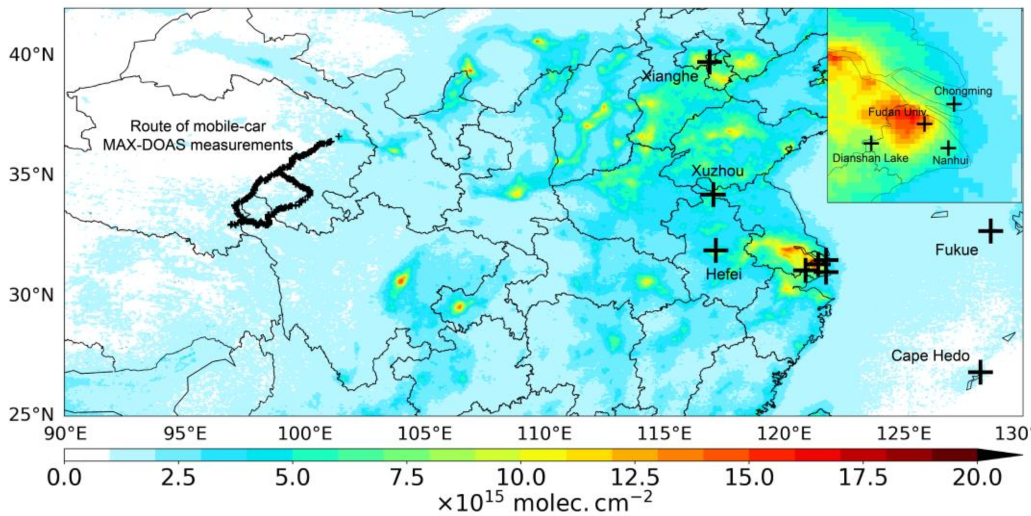

Figure S6. Spatial distribution of ground-based MAX-DOAS sites and the route of mobile-car MAX-DOAS measurements used in this study. Overlaid in the background is the spatial distribution of POMINO-GEMS tropospheric NO_2 VCDs in JJA 2021 on a 0.05° × 0.05° grid.

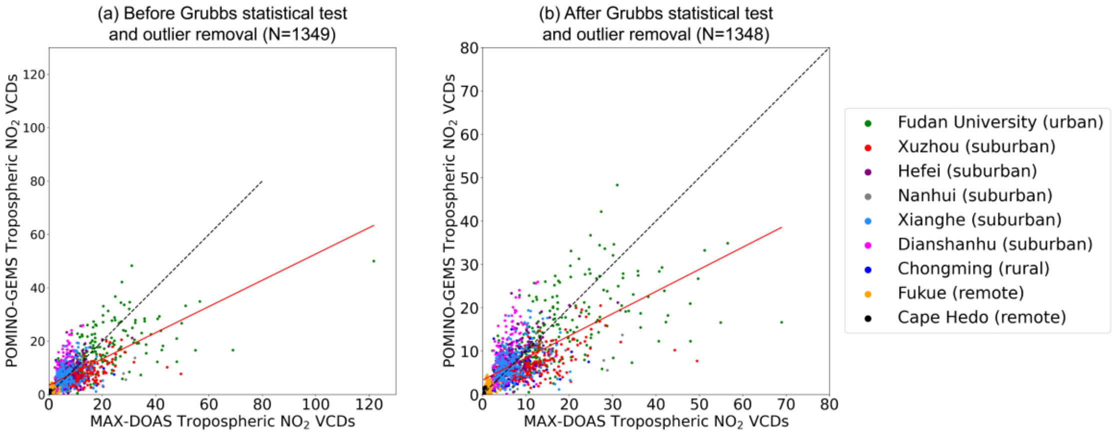

Figure S7. Scatterplots for tropospheric NO_2 VCDs ($\times 10^{15}$ molec. cm^{-2}) between MAX-DOAS and POMINO-GEMS at all GEMS observation hours in JJA 2021 (a) before and (b) after performing Grubbs statistical test and outlier removal. Only one outlier is identified.

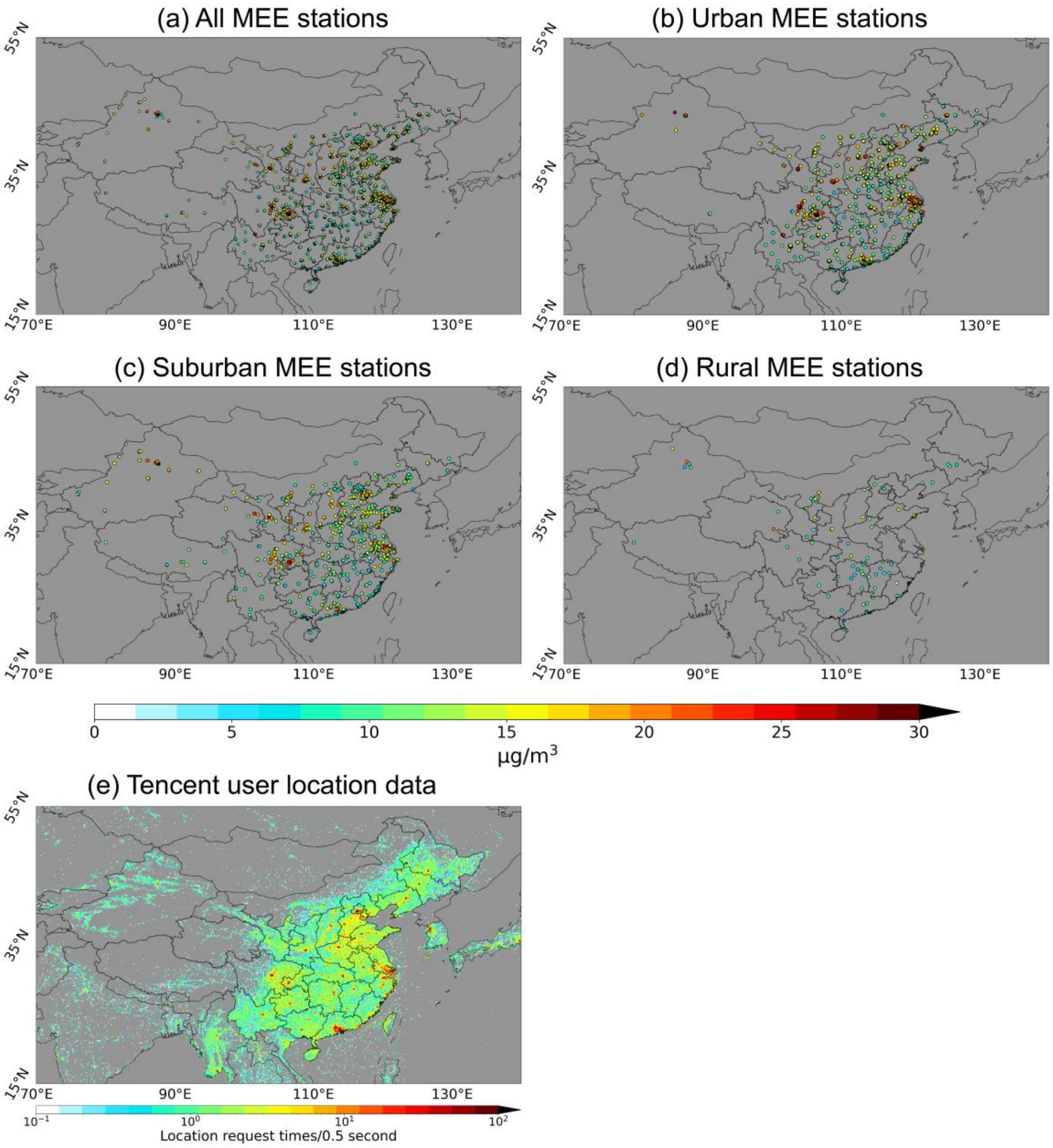

Figure S8. Spatial distribution of mean MEE surface NO_2 concentrations in JJA 2021 at (a) all, (b) urban, (c) suburban and (d) rural sites. The classification is based on (e) mean Tencent user location data from 31 August to 30 September 2021 in China. The regions in grey mean there are no valid observations.

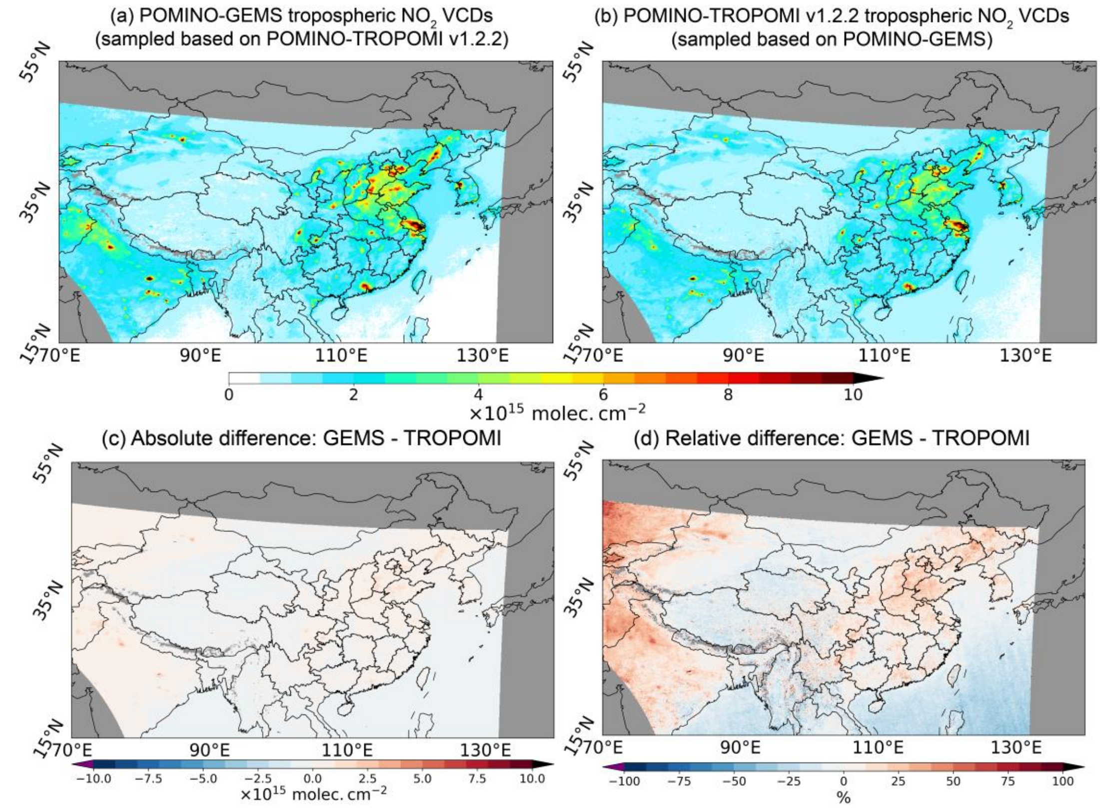

Figure S9. Spatial distribution of (a) POMINO-GEMS and (b) POMINO-TROPOMI v1.2.2 tropospheric NO_2 VCDs on a 0.05° × 0.05° grid in JJA 2021. (c) and (d) are absolute and relative differences of POMINO-GEMS tropospheric NO_2 VCDs from those of POMINO-TROPOMI v1.2.2, respectively. Data are sampled from locations and times with valid data in both POMINO-GEMS and POMINO-TROPOMI v1.2.2. The regions in grey mean there are no valid observations.

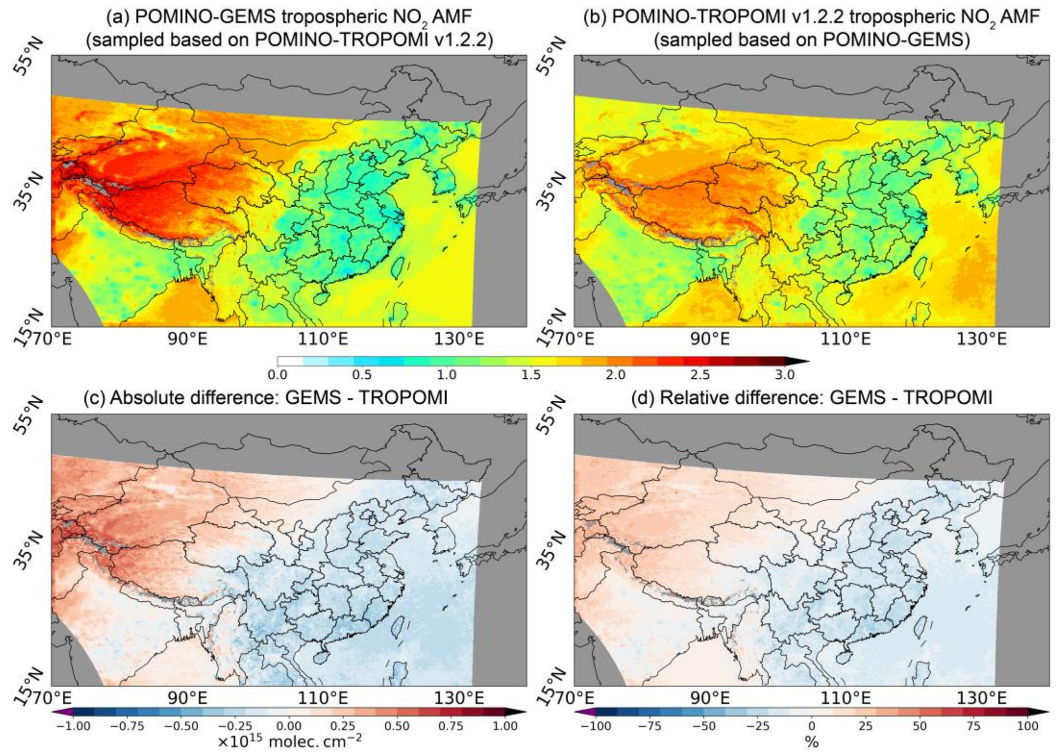

Figure S10. Spatial distribution of (a) POMINO-GEMS and (b) POMINO-TROPOMI v1.2.2 tropospheric NO_2 AMFs on a 0.05° × 0.05° grid in JJA 2021. (c) and (d) are absolute and relative differences of POMINO-GEMS tropospheric NO_2 AMFs from those of POMINO-TROPOMI v1.2.2, respectively. Data are sampled from locations and times with valid NO_2 VCD data in both POMINO-GEMS and POMINO-TROPOMI v1.2.2. The regions in grey mean there are no valid NO_2 observations.

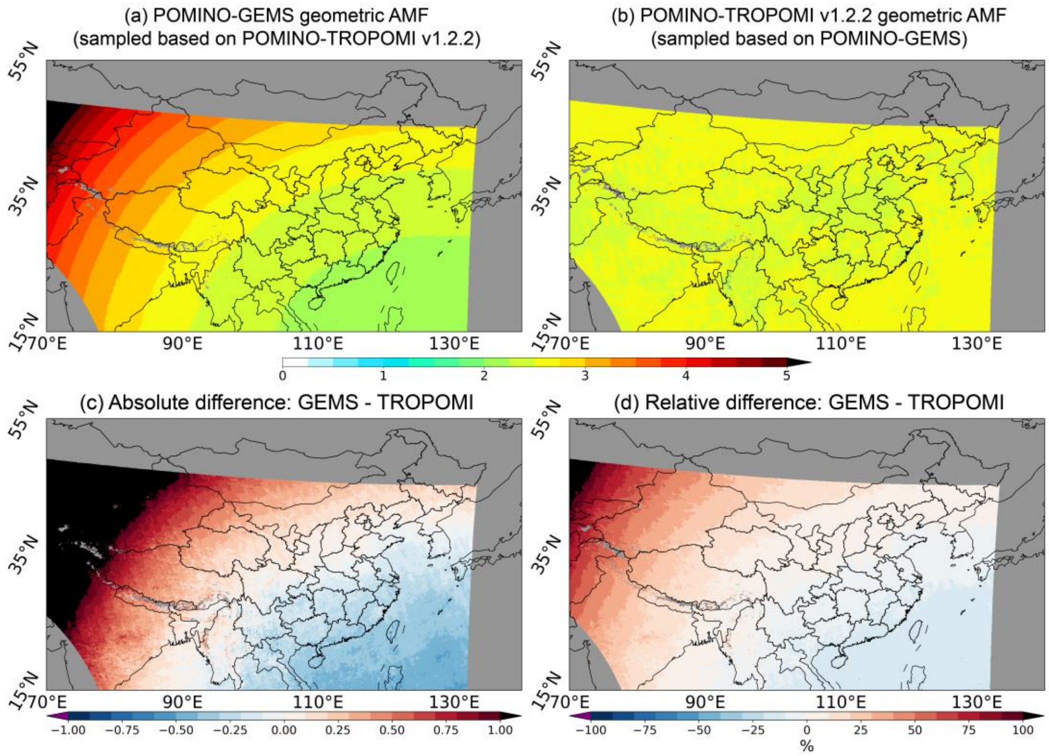

Figure S11. Spatial distribution of (a) POMINO-GEMS and (b) POMINO-TROPOMI v1.2.2 geometric AMFs on a 0.05° × 0.05° grid in JJA 2021. (c) and (d) are absolute and relative differences of POMINO-GEMS geometric AMFs from those of POMINO-TROPOMI v1.2.2, respectively. Data are sampled from locations and times with valid NO_2 VCD data in both POMINO-GEMS and POMINO-TROPOMI v1.2.2. The regions in grey mean there are no valid NO_2 observations.

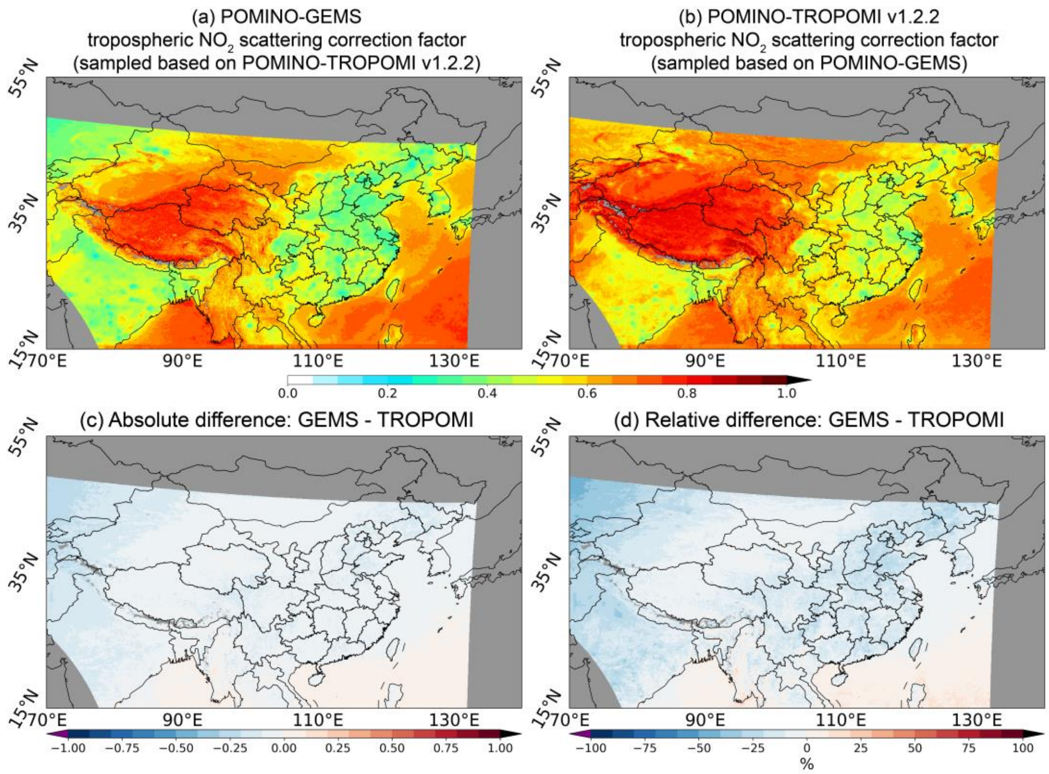

Figure S12. Spatial distribution of (a) POMINO-GEMS and (b) POMINO-TROPOMI v1.2.2 tropospheric NO_2 scattering correction factors on a 0.05° × 0.05° grid in JJA 2021. (c) and (d) are absolute and relative differences of POMINO-GEMS tropospheric NO_2 scattering correction factors from those of POMINO-TROPOMI v1.2.2, respectively. Data are sampled from locations and times with valid NO_2 VCD data in both POMINO-GEMS and POMINO-TROPOMI v1.2.2. The regions in grey mean there are no valid NO_2 observations.

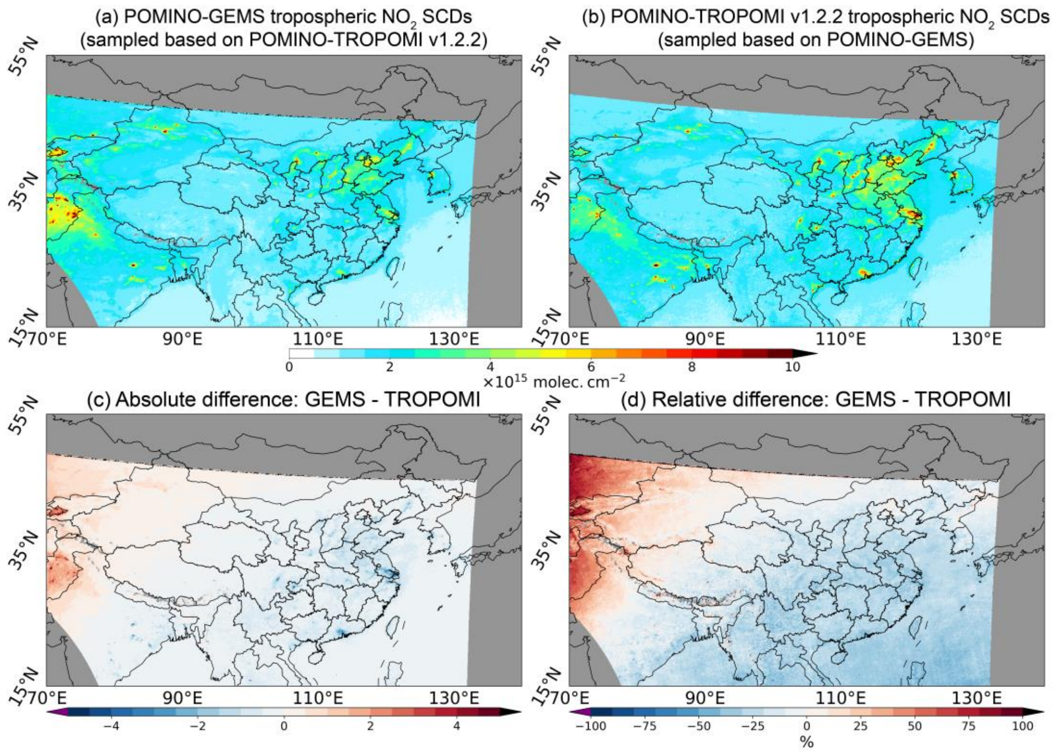

Figure S13. Spatial distribution of (a) POMINO-GEMS and (b) POMINO-TROPOMI v1.2.2 tropospheric NO_2 SCDs on a 0.05° × 0.05° grid in JJA 2021. (c) and (d) are absolute and relative differences of POMINO-GEMS tropospheric NO_2 SCDs from those of POMINO-TROPOMI v1.2.2, respectively. Data are sampled from locations and times with valid NO_2 VCD data in both POMINO-GEMS and POMINO-TROPOMI v1.2.2. The regions in grey mean there are no valid NO_2 observations.

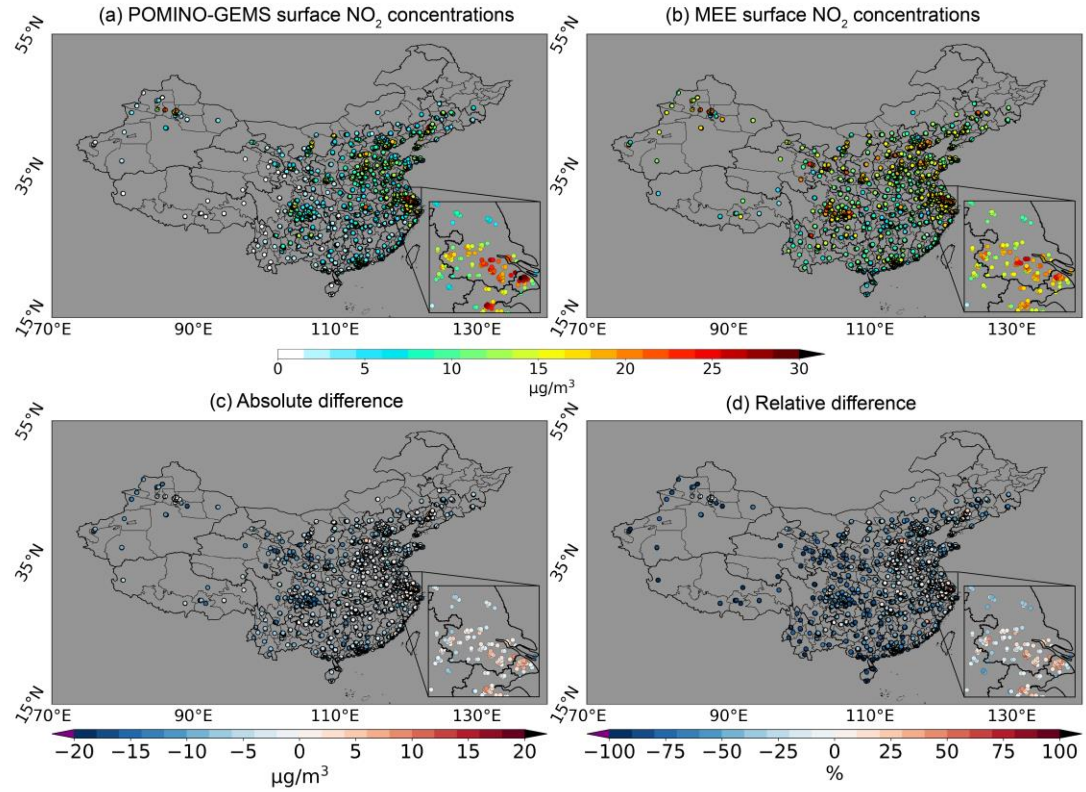

Figure S14. Evaluation of POMINO-GEMS derived surface NO_2 concentrations. Mean surface NO_2 concentrations (a) derived from POMINO-GEMS VCDs and (b) taken from MEE measurements in JJA 2021. Panels (c) and (d) are the absolute and relative differences of POMINO-GEMS relative to MEE. The sub-figures show a zoomed-in map around the Yangtze River Delta (YRD) region (118-122°E, 30-34°N).

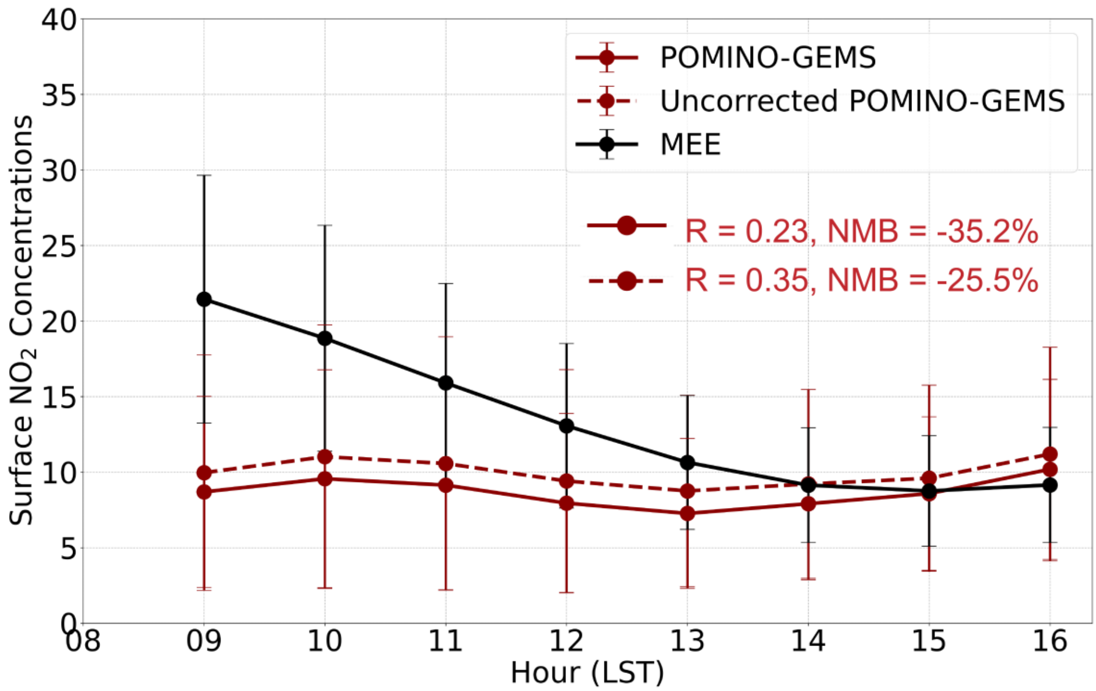

Figure S15. Diurnal variation of hourly surface NO_2 concentrations (μg m^{-3}) of MEE (back line), POMINO-GEMS with TROPOMI correction (red solid line) and without TROPOMI correction (red dashed line) using daily GEOS-Chem column-to-surface ratios in JJA 2021. The error bars denote the standard deviation of MEE and POMINO-GEMS derived surface NO_2 concentrations at each hour in JJA 2021, respectively. Values for diurnal correlation and mean NMB of POMINO-GEMS relative to MEE data are shown.

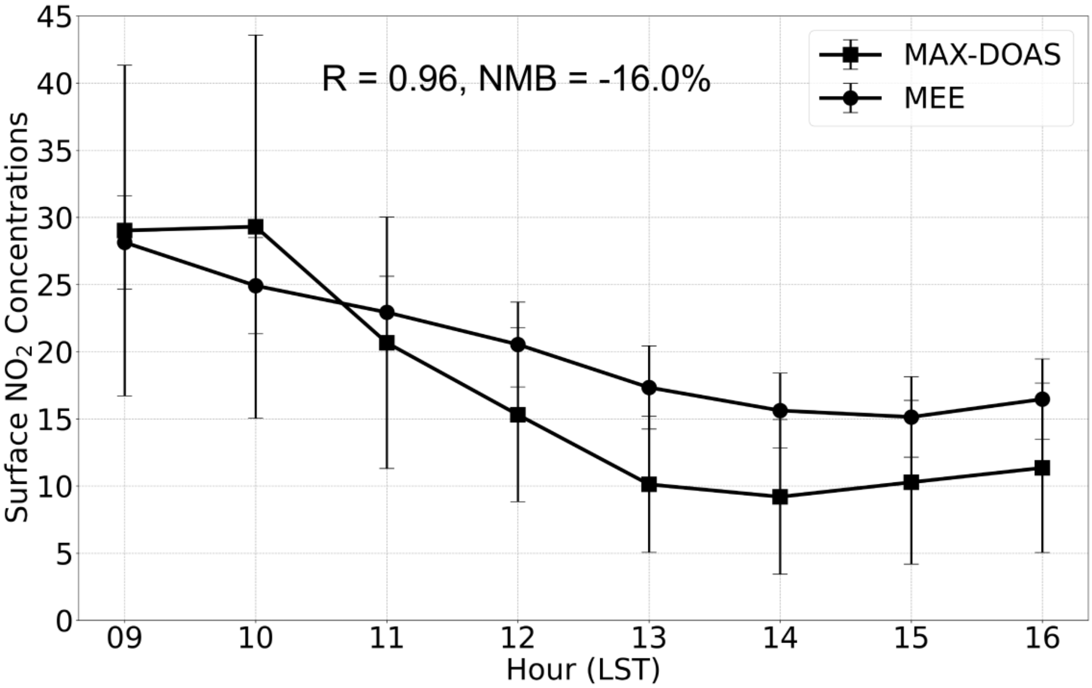

Figure S16. Diurnal variation of hourly surface NO_2 concentrations (μg m^{-3}) for MEE (circle marks) and MAX-DOAS (square marks) in JJA 2021. The error bars denote the standard deviation of MEE and MAX-DOAS derived surface NO_2 concentrations at each hour in JJA 2021, respectively. Values for diurnal correlation and mean NMB of MAX-DOAS derived surface NO_2 concentrations relative to MEE data are shown.

References

Bogumil, K., Orphal, J., Homann, T., Voigt, S., Spietz, P., Fleischmann, O. C., Vogel, A., Hartmann, M., Kromminga, H., Bovensmann, H., Frerick, J., and Burrows, J. P.: Measurements of molecular absorption spectra with the SCIAMACHY pre-flight model: instrument characterization and reference data for atmospheric remote-sensing in the 230–2380 nm region, Journal of Photochemistry and Photobiology A: Chemistry, 157, 167-184, https://doi.org/10.1016/S1010-6030(03)00062-5, 2003.

Chance, K. and Kurucz, R. L.: An improved high-resolution solar reference spectrum for earth's atmosphere measurements in the ultraviolet, visible, and near infrared, Journal of Quantitative Spectroscopy and Radiative Transfer, 111, 1289-1295, https://doi.org/10.1016/j.jqsrt.2010.01.036, 2010.

Chance, K. V. and Spurr, R. J. D.: Ring effect studies: Rayleigh scattering, including molecular parameters for rotational Raman scattering, and the Fraunhofer spectrum, Appl. Opt., 36, 5224-5230, 10.1364/AO.36.005224, 1997.

Choi, Y., Kanaya, Y., Takashima, H., Irie, H., Park, K., and Chong, J.: Long-Term Variation in the Tropospheric Nitrogen Dioxide Vertical Column Density over Korea and Japan from the MAX-DOAS Network, 2007–2017, Remote Sensing, 13, 1937, 10.3390/rs13101937, 2021.

Clémer, K., Van Roozendael, M., Fayt, C., Hendrick, F., Hermans, C., Pinardi, G., Spurr, R., Wang, P., and De Mazière, M.: Multiple wavelength retrieval of tropospheric aerosol optical properties from MAXDOAS measurements in Beijing, Atmospheric Measurement Techniques, 3, 863-878, 10.5194/amt-3-863-2010, 2010.

Hendrick, F., Müller, J.-F., Clémer, K., Wang, P., De Mazière, M., Fayt, C., Gielen, C., Hermans, C., Ma, J. Z., Pinardi, G., Stavrakou, T., Vlemmix, T., and Van Roozendael, M.: Four years of ground-based MAX-DOAS observations of HONO and NO₂ in the Beijing area, Atmospheric Chemistry and Physics, 14, 765-781, 10.5194/acp-14-765-2014, 2014.

Kanaya, Y., Irie, H., Takashima, H., Iwabuchi, H., Akimoto, H., Sudo, K., Gu, M., Chong, J., Kim, Y. J., Lee, H., Li, A., Si, F., Xu, J., Xie, P.-H., Liu, W.-Q., Dzhola, A., Postylyakov, O., Ivanov, V., Grechko, E., Terpugova, S., and Panchenko, M.: Long-term MAX-DOAS network observations of NO₂ in Russia and Asia (MADRAS) during the period 2007–2012: instrumentation, elucidation of climatology, and comparisons with OMI satellite observations and global model si, Atmospheric Chemistry and Physics, 14, 7909-7927, 10.5194/acp-14-7909-2014, 2014.

Liu, M., Lin, J., Kong, H., Boersma, K. F., Eskes, H., Kanaya, Y., He, Q., Tian, X., Qin, K., Xie, P., Spurr, R., Ni, R., Yan, Y., Weng, H., and Wang, J.: A new TROPOMI product for tropospheric NO2 columns over East Asia with explicit aerosol corrections, Atmos. Meas. Tech., 13, 4247-4259, 10.5194/amt-13-4247-2020, 2020.

Liu, M., Lin, J., Boersma, K. F., Pinardi, G., Wang, Y., Chimot, J., Wagner, T., Xie, P., Eskes, H., Van Roozendael, M., Hendrick, F., Wang, P., Wang, T., Yan, Y., Chen, L., and Ni, R.: Improved aerosol correction for OMI tropospheric NO2 retrieval over East Asia: constraint from CALIOP aerosol vertical profile, Atmospheric Measurement Techniques, 12, 1-21, 10.5194/amt-12-1-2019, 2019.

Pope, R. M. and Fry, E. S.: Absorption spectrum (380–700 nm) of pure water. II. Integrating cavity measurements, Appl. Opt., 36, 8710-8723, 10.1364/AO.36.008710, 1997.

Serdyuchenko, A., Gorshelev, V., Weber, M., Chehade, W., and Burrows, J. P.: High spectral resolution ozone absorption cross-sections – Part 2: Temperature dependence, Atmos. Meas. Tech., 7, 625-636, 10.5194/amt-7-625-2014, 2014.

Thalman, R. and Volkamer, R.: Temperature dependent absorption cross-sections of O2–O2 collision pairs between 340 and 630 nm and at atmospherically relevant pressure, Physical Chemistry Chemical Physics, 15, 15371-15381, 10.1039/C3CP50968K, 2013.

Vandaele, A. C., Hermans, C., Simon, P. C., Carleer, M., Colin, R., Fally, S., Mérienne, M. F., Jenouvrier, A., and Coquart, B.: Measurements of the NO2 absorption cross-section from 42 000 cm−1 to 10 000 cm−1 (238–1000 nm) at 220 K and 294 K, Journal of Quantitative Spectroscopy and Radiative Transfer, 59, 171-184, https://doi.org/10.1016/S0022-4073(97)00168-4, 1998.

Zhang, R., Wang, S., Zhang, S., Xue, R., Zhu, J., and Zhou, B.: MAX-DOAS observation in the midlatitude marine boundary layer: Influences of typhoon forced air mass, Journal of Environmental Sciences, 120, 63-73, https://doi.org/10.1016/j.jes.2021.12.010, 2022a.

Zhang, S., Wang, S., Xue, R., Zhu, J., Tanvir, A., Li, D., and Zhou, B.: Impact Assessment of COVID-19 Lockdown on Vertical Distributions of NO2 and HCHO From MAX-DOAS Observations and Machine Learning Models, Journal of Geophysical Research: Atmospheres, 127, e2021JD036377, https://doi.org/10.1029/2021JD036377, 2022b.

Zhang, S., Wang, S., Zhang, R., Guo, Y., Yan, Y., Ding, Z., and Zhou, B.: Investigating the Sources of Formaldehyde and Corresponding Photochemical Indications at a Suburb Site in Shanghai From MAX-

DOAS Measurements, Journal of Geophysical Research: Atmospheres, 126, e2020JD033351, https://doi.org/10.1029/2020JD033351, 2021.

Zhu, J., Wang, S., Dao, X., Liu, D., Wang, J., Zhang, S., Xue, R., Tang, G., and Zhou, B.: Comparative observation of aerosol vertical profiles in urban and suburban areas: Impacts of local and regional transport, Science of The Total Environment, 805, 150363, https://doi.org/10.1016/j.scitotenv.2021.150363, 2022.